Inorganic Chemistry

Article

pubs.acs.org/IC

$Fe^{II}(pap\text{-}5NO_2)_2$ and $Fe^{II}(qsal\text{-}5NO_2)_2$ Schiff-Base Spin-Crossover Complexes: A Rare Example with Photomagnetism and Room-Temperature Bistability

Olga Iasco,[†] Eric Rivière,[†] Régis Guillot,[†] Marylise Buron-Le Cointe,[‡] Jean-François Meunier,[§] Azzedine Bousseksou,[§] and Marie-Laure Boillot*[,†]

[†]ICMMO-ECI, UMR CNRS 8182, Université Paris-Sud, 91405 Orsay cedex, France

[‡]IPR, UMR UR1-CNRS 6251, Université de Rennes 1, 35042 Rennes, France

[§]CNRS, LCC, UPR 8241, 31077 Toulouse cedex 4, France

Supporting Information

ABSTRACT: We focus here on the properties of Fe complexes formed with Schiff bases involved in the chemistry of Fe^{III} spin-transition archetypes. The neutral $Fe(pap\text{-}5NO_2)_2$ (**1**) and $Fe(qsal\text{-}5NO_2)_2$·Solv (**2** and **2·Solv**) compounds (**Solv** = $2H_2O$) derive from the reaction of Fe^{II} salts with the condensation products of pyridine-2-carbaldehyde with 2-hydroxy-5-nitroaniline ($Hpap\text{-}5NO_2$) or 5-nitro-salicylaldehyde with quinolin-8-amine ($Hqsal\text{-}5NO_2$), respectively. While the $Fe(qsal\text{-}5NO_2)_2$·Solv solid is essentially low spin (S = 0) and requires temperatures above 300 K to undergo a S = 0 ↔ S = 2 spin-state switching, the $Fe(pap\text{-}5NO_2)_2$ one presents a strongly cooperative first-order transition ($T\downarrow$ = 291 K, $T\uparrow$ = 308 K) centered at room temperature associated with a photomagnetic effect at 10 K (T_{LIESST} = 58 K). The investigation of these magnetic behaviors was conducted with single-crystal X-ray diffraction (**1**, 100 and 320 K; **2**, 100 K), Mössbauer, IR, UV−vis (**1** and **2·Solv**), and differential scanning calorimetry (**1**) measurements. The Mössbauer analysis supports a description of these compounds as Fe^{II} Schiff-base complexes and the occurrence of a metal-centered spin crossover process. In comparison with Fe^{III} analogues, it appears that an expanded coordination sphere stabilizes the valence 2+ state of the Fe ion in both complexes. Strong hydrogen-bonding interactions that implicate the phenolato group bound to Fe^{II} promote the required extra-stabilization of the S = 2 state and thus determines the spin transition of **1** centered at room temperature. In the lattice, the hydrogen-bonded sites form infinite chains interconnected via a three-dimensional network of intermolecular van der Waals contacts and $\pi-\pi$ interactions. Therefore, the spin transition of **1** involves the synergetic influence of electrostatic and elastic interactions, which cause the enhancement of cooperativity and result in the bistability at room temperature.

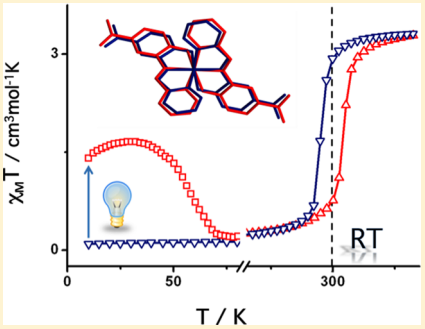

INTRODUCTION

Spin-crossover (SCO) compounds, like valence-tautomeric compounds,[1] belong to a class of labile[2] magnetic materials that exhibit the spin-state switching of their metal ion under various stimuli.[1,3] The vibronic nature of both processes occasions a strong environment dependence of properties, as manifested by low cooperativity up to hysteretic transformations of solids. The cooperative character, a critical feature for the design of molecular memory devices, is related to the solid elastic properties.[1,3] Electrostatic contributions are also considered as relevant peculiarities to promote cooperative and bistable behaviors in SCO and charge-transfer solids.[4] The technological potentialities of these materials have triggered research efforts toward new bistable SCO materials, their downsizing, and processing.[1,5] Today, such bistable behaviors are scarcely reported for Fe^{III} compounds[6,7] but are well-documented for Fe^{II} ones,[1,8−10] and only a limited set of molecular compounds meets the criteria of two stable (or metastable) states at room temperature (RT).[9,10] The control of functionalities (magnetic, structural, etc.) by light is also an important topic for SCO solids. The trapping of the high-spin (HS) metastable form may be achieved at low temperature from the photoexcitation of the low-spin (LS) form,[3] according to the light-induced excited spin-state trapping (LIESST). This photoswitching effect was mainly reported for $[Fe^{II}N_6]$ compounds but also for a few $[Fe^{II}N_4O_2]$[11] or $[Fe^{III}N_4O_2]$[6e,7,12] SCO compounds. Changes of electronic properties and structural rearrangements associated with the spin-state photoswitching are presently scrutinized in real time with ultrafast optical and X-ray techniques on crystals and nanocrystals.[13]

As the charge distributions at the intra- and intermolecular levels impact the SCO, we have undertaken to compare their importance in $[FeN_4O_2]$ complexes isolated with Fe^{II}/Fe^{III} and Schiff-base ligands that represents a common SCO environment for both metal ions.

We report here the syntheses, crystalline structures, differential scanning calorimetry (DSC), IR, UV−vis, Mössbauer,

Received: November 10, 2014
Published: January 15, 2015

DOI: 10.1021/ic5027043
Inorg. Chem. 2015, 54, 1791−1799

and magnetic investigations of two polar Fe^{II} complexes incorporating the Hpap and Hqsal ligands (Scheme 1), first

Scheme 1. Protonated Form of the Tridentate Ligands

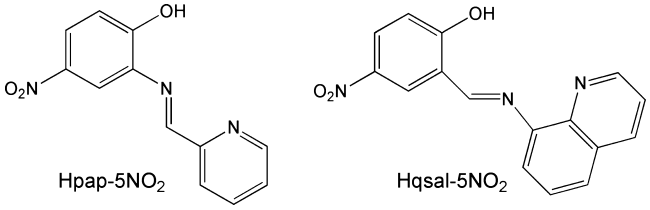

employed in SCO $[Fe^{III}(L)_2]^+$ salts by Oshio,[14] substituted with an electron-withdrawing NO_2 substituent. This investigation shows that the spin-state conversion is preserved in both compounds and that a hysteresis of a few K width is observed at ca. room temperature in the $Fe^{II}(pap\text{-}5NO_2)_2$ system.

EXPERIMENTAL SECTION

Syntheses. All chemicals and solvents were used as received. All manipulations were performed under argon atmosphere using Schlenk techniques or glovebox. The NMR spectra were recorded at 250 MHz on a Bruker DRX spectrometer with deuterated dimethyl sulfoxide (DMSO-d_6) and $CDCl_3$ solutions. The chemical shifts were referenced to the signal of tetramethylsilane.

*2-Hydroxy-5-nitrophenyl-(2-pyridyl)-methaneimine (**Hpap-5NO$_2$**).* A mixture of pyridine-2-carbaldehyde (535 mg, 5 mmol) and 2-hydroxy-5-nitroaniline (770 mg, 5 mmol) in absolute methanol (10 cm^3) was refluxed for 30 min. Sodium methoxide (270 mg, 5 mmol) in absolute methanol (10 cm^3) was added. Refluxing was continued for 10 min. The mixture filtered on a glass frit gives a yellow product. The solid was washed with methanol and dried under vacuum. Yield: 61%. ^1H NMR (DMSO-d_6): δ 9.05 (s, 1H), 8.72 (d, 1H), 8.28 (d, 1H), 8.05−7.93 (m, 3H), 7.53 (m, 1H), 6.89 (d, 1H).

*(8-Quinolyl)-5-nitrosalicylaldimine (**Hqsal-5NO$_2$**).*[15] A mixture of 5-nitrosalicylaldehyde (835 mg, 5 mmol) and quinolin-8-amine (720 mg, 5 mmol) in absolute methanol (25 cm^3) was refluxed for 4 h. The mixture was cooled to room temperature, and an orange product was collected by filtration and dried under vacuum. Yield: 89%. ^1H NMR ($CDCl_3$): δ 9.11 (s, 1H), 9.03 (m, 1H), 8.46 (d, 1H), 8.30−8.23 (m, 2H), 7.84 (m, 1H), 7.66 (s, 1H), 7.65 (d, 1H), 7.54 (m, 1H), 7.10 (d, 1H).

*$Fe^{II}(pap\text{-}5NO_2)_2$ (**1**).* A 20 mL aliquot of methanolic suspension of Hpap-5NO_2 (243 mg, 1 mmol) and triethylamine (140 μL, 1 mmol) was slowly added to 10 mL of methanolic solution containing $Fe(BF_4)_2{\cdot}6H_2O$ (169 mg, 0.5 mmol). After 1 h of stirring, a dark precipitate was filtered, washed with methanol, and dried under vacuum. Yield: 61% (based on Fe). Elemental analysis (%) Calcd (Found) for $C_{24}H_{16}O_6N_6Fe$: C, 53.35 (52.15); H, 2.99 (2.84); N, 15.56 (15.04)%. HR-ESI$^+$: calculated for $[Fe^{II}(pap\text{-}5NO_2)_2]^+$ + H 541.0554; found, 541.0534; $[Fe^{II}(pap\text{-}5NO_2)_2]^+$ + Na 563.0373; found, 563.0364. Dark violet needlelike crystals of **1** suitable for X-ray analysis were obtained after 4 d by slow diffusion of a methanolic solution of $Fe(BF_4)_2{\cdot}6H_2O$ into a dichloromethane solution of deprotonated Hpap-5NO_2.

*$Fe^{II}(qsal\text{-}5NO_2)_2{\cdot}Solv$ (**2** or **2·Solv**, with Solv = $2H_2O$).* A 20 mL aliquot of methanolic suspension of Hqsal-5NO_2 (293 mg, 1 mmol) and triethylamine (140 μL, 1 mmol) was slowly added to 10 mL of methanolic solution containing $Fe(BF_4)_2{\cdot}6H_2O$ (169 mg, 0.5 mmol). After 1 h of stirring, a dark precipitate was filtered, washed with methanol, and dried under vacuum. Yield: 80% (based on Fe). Elemental analysis (%) Calcd (Found) for $C_{32}H_{24}O_8N_6Fe$ (**2·Solv** with Solv = $2H_2O$): C, 56.82 (55.30); H, 3.58 (3.16); N, 12.42 (12.14)%. HR-ESI$^+$: calculated for $[Fe^{II}(qsal\text{-}5NO_2)_2]^+$ 640.0789; found, 640.0777. The thermograms (Figure S1 in Supporting Information) show a loss of weight with a plateau at ∼65 °C (Found 5−6%, Calcd for two water molecules 5.47%) and a reversible hydration of the thermally treated sample after exposure (2 h) to ambient atmosphere. Dark violet needlelike crystals of **2** suitable for X-ray analysis were obtained after 4 d by slow diffusion of a methanolic solution of $Fe(BF_4)_2{\cdot}6H_2O$ into an acetone solution of deprotonated Hqsal-5NO_2. Unfortunately, the attempts made for obtaining single crystals of the dihydrated sample **2·Solv** were unsuccessful.

X-ray Data Collection and Structure Refinement. The single-crystal X-ray diffraction data were collected by using a Kappa X8 APPEX II Bruker diffractometer with graphite-monochromated Mo Kα radiation (λ = 0.710 73 Å) at various temperatures. A summary of the crystallographic data and structure refinement are given in Table 1.

For 100 K, the single crystals were mounted on a Mitigen Kapton loop with Paratone-N (Hampton Research) as cryoprotectant and then rapidly frozen in a nitrogen-gas stream at 100 K. For 320 K, the single crystal was glued on support diffraction. The temperature of the crystal during the data collection was controlled with an Oxford Cryosystems Series 700 instrument. The data were corrected for Lorentz polarization and absorption effects.

The structures were solved by direct methods using SHELXS-97[16] and refined against F^2 by full-matrix least-squares techniques using SHELXL-97[17] with anisotropic displacement parameters for all non-hydrogen atoms. Hydrogen atoms were located on a difference Fourier

Table 1. Crystal Data and Structure Refinement Parameters

	$Fe^{II}(pap\text{-}5NO_2)_2$ (**1**)		$Fe^{II}(qsal\text{-}5NO_2)_2$ (**2**)
chemical formula	$C_{24}H_{16}FeN_6O_6$		$C_{32}H_{20}FeN_6O_6$
formula weight (g/mol)	540.28		640.39
temperature (K)	320(2)	100(1)	100(1)
crystal system	monoclinic	monoclinic	orthorhombic
space group	*C*2/*c*	*C*2/*c*	*Pcca*
a (Å)	23.267(18)	22.948(2)	19.2422(13)
b (Å)	8.902(7)	9.0760(8)	10.4155(9)
c (Å)	11.967(9)	11.9420(9)	12.9086(10)
β (deg)	114.198(13)	119.587(2)	90.00
V (Å^3), *Z*	2261(3), 4	2162.9(3), 4	2587.1(3), 4
density (calc) (g·cm^{-3})	1.587	1.659	1.644
abs. coefficient (mm^{-1})	0.670	0.756	0.647
goodness-of-fit on F^2	1.016	1.041	1.036
final *R* indices [$I > 2\sigma(I)$]	*R*1 = 0.0431; *wR*2 = 0.0992	*R*1 = 0.0465; *wR*2 = 0.0833	*R*1 = 0.0547; *wR*2 = 0.1333
R indices (all data)	*R*1 = 0.0718; *wR*2 = 0.1130	*R*1 = 0.0881; *wR*2 = 0.0961	*R*1 = 0.0902; *wR*2 = 0.1557
$\Delta\rho_{min}$ and $\Delta\rho_{max}$ (e Å^{-3})	−0.411; 0.280	−0.457; 0.420	−0.517; 0.797

DOI: 10.1021/ic5027043
Inorg. Chem. 2015, 54, 1791−1799

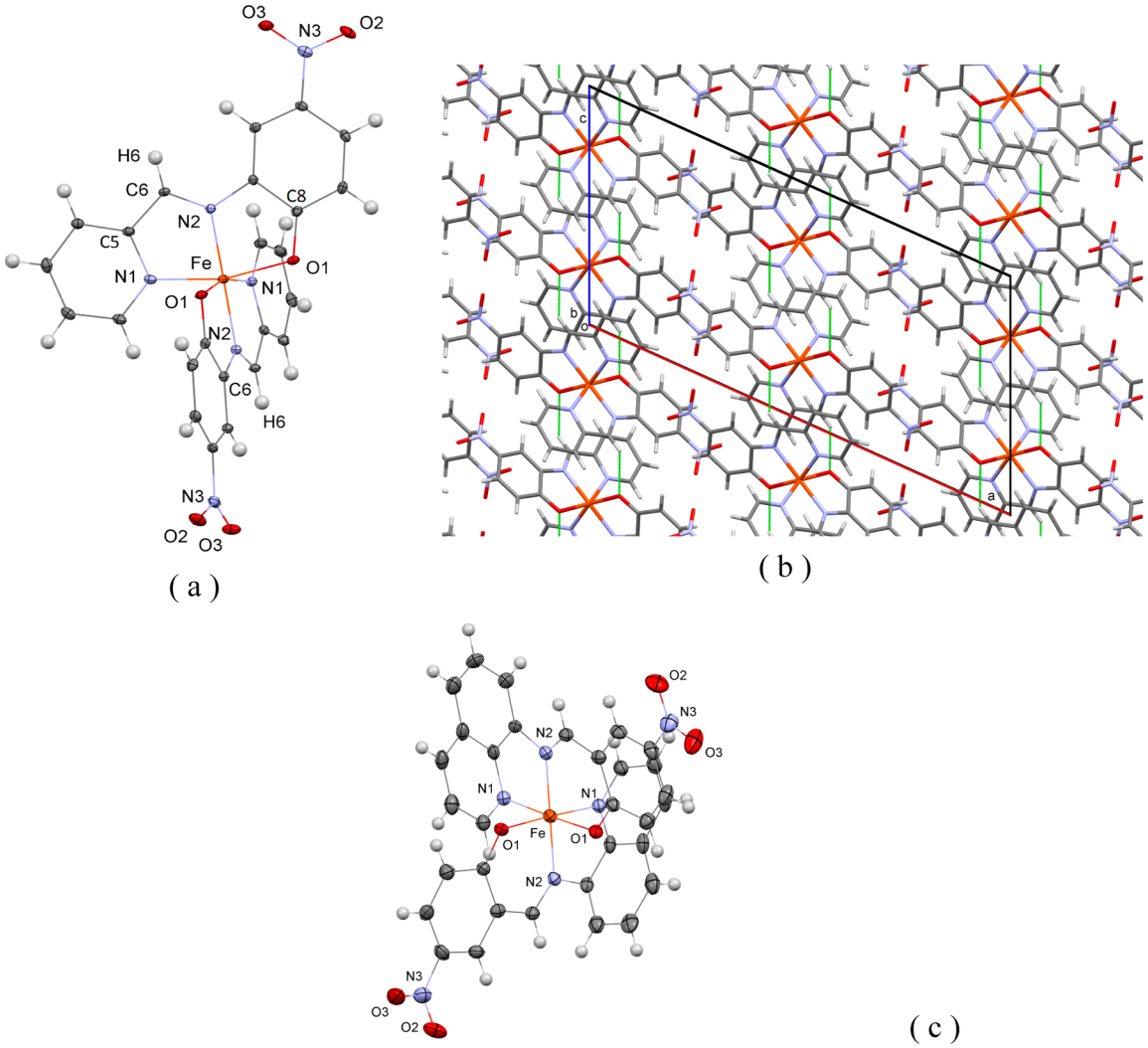

Figure 1. (a) ORTEP views of **1** at 100 K. (b) Packing of **1** along *b* axis (320 K). In green, are shown the hydrogen bonds corresponding to distances shorter than $\Sigma(R^{\text{van der Waals}}) - 0.3$ Å. (c) ORTEP views of **2** at 100 K.

map and introduced into the calculations as a riding model with isotropic thermal parameters. All calculations were performed by using the Crystal Structure crystallographic software package WINGX.[18]

Powder X-ray Diffraction Measurements. The X-ray diffraction (XRD) patterns were recorded at RT on powders deposited on aluminum plate, using a Philipps Panalytical X'Pert Pro MPD powder diffractomer at Cu Kα radiation equipped with a fast detector within the 6−37° 2θ range. Figures S2 and S3 (in the Supporting Information) show the superposition of diffractograms recorded at RT for **1** and **2·Solv** in the form of polycrystalline powders and those calculated from the single-crystal structures of **1** and **2**.

Spectroscopic Measurements. FT-IR spectra (see Figures S4 and S5 in the Supporting Information) were carried out on a PerkinElmer spectrometer (Spectrum 100) equipped with the Eurolabo variable-temperature cell (21525, KBr windows) and Specac temperature controller (20120). The measurements were performed on KBr pellets (approximately 3 mg of fresh crystallites of compound dispersed without any grinding in ca. 97 mg of KBr, this latter being previously ground) in the 300−4000 cm^{-1} range between 223 and 463 K (**1**) or at RT (**2·Solv**). Solid-state UV−vis spectra were measured in the range of 200−2000 nm on a CARY 5000 double-beam spectrophotometer with the same Eurolabo variable-temperature cell (quartz windows) and Specac temperature controller. The sample was prepared in a similar way as for the FT-IR study: approximately 1 mg of fresh crystallites of **1** or **2·Solv** dispersed without any grinding in ca. 99 mg of KBr, this latter being previously ground. This sample preparation aimed at minimizing the formation of crystalline defects that alter the SCO characteristics.

Magnetic Measurements. Magnetic susceptibility data were collected using a Quantum Design SQUID magnetometer (MPMS5S Model) calibrated against a standard palladium sample. The magnetic susceptibility values were corrected from the diamagnetism of the molecular constituents and of the sample holder. The measurement was carried out with (i) small crystals of $Fe(pap\text{-}5NO_2)_2$ (checked by IR and unit-cell analysis), a polycrystalline powder (XRD pattern, Figure S2 in Supporting Information) or (ii) a freshly synthesized powder of $Fe(qsal\text{-}5NO_2)_2 \cdot 2H_2O$ (XRD pattern, Figure S3 in Supporting Information). The latter was selected as our attempts to isolate a significant amount of single crystals of **2** failed.

For photoexcitation experiments, the magnetometer was equipped with an optical fiber (UV-grade fused silica) connected to a Nd:YAG pulsed laser Surelite-OPO Plus (energy (at peak) 10 mJ, repetition rate 10 Hz, tuning range of 410−2630 nm, signal and idler pulsewidth 3−5 ns). In situ excitations were performed on a small quantity of powder deposited on adhesive tape with λ = 750 nm or λ = 900 nm (40 mW/cm^2). The samples (**1** and **2·Solv**) were prepared by careful size reduction of the polycrystalline powders (XRD patterns in Figures S2 and S3 in the Supporting Information).

Mössbauer Measurements. Variable-temperature Mössbauer spectra were collected on a constant-acceleration conventional spectrometer with a 0.30 GBq source of ^{57}Co (Rh matrix) in the temperature range of 80−315 K, using a MD306 Oxford cryostat, with

DOI: 10.1021/ic5027043
Inorg. Chem. 2015, 54, 1791−1799

the thermal scanning being monitored by an Oxford ITC4 servo control device (0.1 K). The absorber was a sample of ca. 40−50 mg of microcrystalline powder that was enclosed in a 20 mm diameter cylindrical plastic sample holder, the size of which was determined to optimize the absorption. The hyperfine parameters and their standard deviations of statistical origin (given in parentheses) were obtained by least-squares fitting to Lorentzian lines. The isomer shift values (δ) are given with respect to metallic iron at RT. The samples of **1** (small single crystals) and **2·Solv** (polycrystalline powder) were strictly the same as those studied by magnetic measurements.

Thermal Gravimetric Analysis. The measurement was carried out with a TGA analyzer (TA Instruments-water LLC, SDT Q600) at a rate of 5 °C min^{-1}. The sample (**2·Solv**, ∼10 mg) was maintained under an air flow (100 cm^3 min^{-1}).

Differential Scanning Calorimetry Measurements. The DSC measurements were performed with a Q-20a TA Instrument using aluminum hermetic pans. Temperature varied between −80 °C and +100 °C with both heating and cooling rates of 5 K·min^{-1}. Indium value was used for calibration of ΔH.

RESULTS AND DISCUSSION

New Fe(pap-5NO_2)$_2$ (**1**) and Fe(qsal-5NO_2)$_2$ (**2**) complexes were isolated in the form of dark violet single crystals from the reaction of Fe^{II} cations with deprotonated Schiff-bases [pap-5NO_2]$^-$ and [qsal-5NO_2]$^-$, respectively.

Description of Structures. The crystal structures were determined at 100 (**1** and **2**) and 320 K (**1**) corresponding to the LS and HS phases, respectively. The asymmetric unit of **1** and **2** contains one-half of complex centered on a 2-fold rotation proper axis. The space group of **1** is preserved upon heating to 320 K, a feature that indicates the isostructural nature of the first-order phase transition coupled to the spin-state switching characterized below. The monoclinic unit cell of **1** evolves with strong changes along the *b* and *a* axes (in opposite direction, -1.92×10^{-2} and 1.39×10^{-2}, respectively) and of β angle (-4.5×10^{-2}) that reflect both the thermal expansion and spin transition ($\Delta V/V$ = 4.5%).

The molecular structures of **1** and **2** show the [N_4O_2] asymmetrical environment of the metal ion chelated by ligands (with two five-membered (**1**) or five-membered and six-membered (**2**) chelate cycles) and the NO_2 groups located close to the aromatic planes (Figure 1a,c and Figures S6 and S7 in the Supporting Information). At 100 K, the set of bond lengths (angles) of **1** and **2** (Table 2) are similar to those assigned to LS Fe^{II} species in [Fe(qnal)$_2$]·CH_2Cl_2 (Hqnal = *N*-(8′-quinolyl)-2-hydroxy-1-naphthaldimine) or [Fe^{II}(3-X,5-NO_2-sal-N(1,4,7,10))] compounds (Schiff base formed by condensation of 5-nitrosalicylaldehyde with tetraazadecane).[11a,19,20,21c] The superposition of **1** (Figure S8 in the Supporting Information) at 100 and 320 K shows the large reorientation of the rigid backbone of pap with respect to the Fe atom resulting from the change of spin (characterized below), the intrinsic distortions (associated with the five-membered chelate cycles), and the marked change of hydrogen bonds (Figure S9 in Supporting Information). The molecular parameters of **1** vary accordingly (bond length LS (HS), Fe−O = 1.98 (2.07) Å; Fe−N_{im} = 1.88 (2.12) Å; Fe−N_{py} = 1.96 (2.22) Å, distortion Σ = 66.5 (128.3)°) and are very typical for Schiff-base Fe^{II} complexes (Table S1 in the Supporting Information).[10b,11a,21a,b]

One intriguing feature is the length of Fe−O_1 bonds that indicates weak interactions between the metal ion and negatively charged phenol groups. This bond, which is very strong in Fe^{III} analogues,[6,7] is here undermined by hydrogen-bonding interactions (C_8−O_1···H_6−C_6^{imine} = 2.34 (320 K) and 2.38 Å (100 K)) (Tables S2 and S3 in the Supporting Information). This weakens the electron-releasing character[6h,10a,c] of O_1 atoms (especially for HS ones) but as a counterpart, reinforces the C_6=N_2 bond by donor-inductive effect.

Table 2. Selected Bond Distances and cis Bond Angles of 1 and 2

	1, 100 K	**1**, 320 K	**2**, 100 K
Fe O1	1.9756(16)	2.073(2)	1.943(3)
Fe N2	1.8841(16)	2.122(2)	1.932(4)
Fe N1	1.9570(19)	2.223(3)	1.944(4)
C5 C6	1.444(3)	1.455(4)	
C6 N2[a]	1.299(3)	1.272(3)	1.289(6)
C8 O1[a]	1.303(2)	1.299(3)	1.281(6)
O1 Fe O1	87.63(9)	97.69(15)	89.6(2)
O1 Fe N2	96.64(7)	111.56(9)	93.94(16)
O1 Fe N2	83.97(7)	77.17(9)	87.47(15)
O1 Fe N1	91.70(7)	93.13(10)	89.83(15)
N2 Fe N1	81.52(7)	74.05(9)	83.68(17)
N2 Fe N1	97.90(8)	96.80(9)	94.93(17)
N1 Fe N1	92.62(11)	89.95(14)	90.8(2)
Fe−L (Å)[b]	1.939	2.139	1.940
ζ (Å)[b]	0.110	0.167	0.015
Σ (deg)[b]	66.5	128.3	37.0

[a]In case of **2**, C6 N2 and C8 O1 were replaced by C10 N2 and C12 O1, respectively. [b]Fe−L = (1/6) Σd_{Fe-L_i}, $\zeta = \Sigma |d_{Fe-L} - d_{Fe-L_i}|$, $\Sigma = \Sigma |90 - \phi i|$

The charge distribution in these complexes may be questioned as pyridine−diimine or phenolamine involved in the chemistry of ligands are known as redox-active groups reacting with transition metal ions and changing their valence. We reported in Table 2 the values of C^{py}−C^{im}, C^{im}−N^{im}, and C−O^{ph} (with py = pyridine, im = imine, ph = phenolate) that are structural markers[22,23] for analyzing these effects. The C−O bond lengths in **1** (≥1.299(3) Å) or **2** (1.281(6) Å) are lower than those characterizing phenolate groups, especially in case of **2** at 100 K, a feature that might suggest some phenoxyl character (phenolate, 1.33−1.35 Å and phenoxyl, 1.25−1.29 Å from refs 7c and 22). The C^{im}−N^{im} bond distances fall in the range corresponding to imine groups (1.28−1.31 Å) except in the case of **1** at 320 K.[23] The values observed for C^{py}−C^{im} in **1** approach those characterized either for the [Fe^{III}(pap)$_2$]BF_4 or $Mn^{III}(L^{-\cdot})_2$ compounds ($L^{-\cdot}$ = monoreduced pyridine−diimine ligand).[7c,23] Therefore, this analysis shows some discrepancies, but no clear tendency emerges for justifying open-shell ligands and an Fe^{III} metal ion. This hypothesis is ruled out by the Mössbauer investigation (see below) of both compounds (hereafter designed as Fe^{II} compounds). In view of the supramolecular C_8−O_1···H_6−C_6^{im} interaction, involving all these groups in **1**, we suggest that the present anomalies might be induced by the related changes of their structural and electronic characteristics.

Concerning the organization in the lattice (Figure 1b), the so-interacting sites form infinite chains along *c* axis that are packed via an extensive three-dimensional (3D) network of moderate van der Waals and π-stacking interactions both in the LS and HS phase. In the case of **2** (Figure S10 and Tables S4 and S5 in the Supporting Information), the arrangement of neutral complexes is stabilized by a set of moderate 3D contacts involving noncoordinated atoms and weak π-stacking interactions.

DOI: 10.1021/ic5027043
Inorg. Chem. 2015, 54, 1791−1799

Optical Properties. Absorption spectra were collected with crystallites of **1** and **2·Solv** dispersed in KBr pellets. Both samples present at RT similar absorption bands localized in the vis–NIR range (Figure S11 in the Supporting Information). Figure 2 shows the spectral evolution between 223 and 373 K

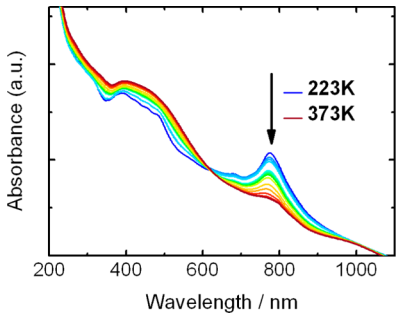

Figure 2. UV–vis spectra of crystallites of **1** (dispersed in KBr) monitored as a function of temperature between 223 (LS, blue), 306–313 (~T↑, green) and 373 (HS, brown) K.

attributed to the thermal spin-state switching of the Fe^{II} ion in **1**. The 771 nm band (with a shoulder at 687 nm) observed at low temperature can be assigned to the LS species as the intensity markedly decreases by heating the sample to 373 K. Conversely, the increase of intensity observed below ca. 612 nm (pseudoisosbestic point) is associated with the formation of HS complexes (unresolved absorption band at ca. 540 nm). The spreading of spectral changes over a range of temperature, which contrasts with the abrupt transition in Figure 4, reveals the influence of the solid encapsulation in a KBr pellet and the relationship between crystallinity and cooperativity.[24]

It is notable that the very broad feature (between 390 and 470 nm) measured at any temperature includes an absorption band of the Hpap-5NO_2 chromophore (Figure S12 in the Supporting Information). Considering the molar extinction coefficient of the latter (4.6×10^3 M^{-1} cm^{-1} at 384 nm in *n*-butanol) and the relative intensities here observed in NIR and visible regions, we can discard the hypothesis of metal-centered transitions[1,3] ($\varepsilon \leq 1 \times 10^2$ mol^{-1} L cm^{-1}) as being responsible for 771 or 540 nm absorption bands and the dark color of **1**. Consistently with the literature on Schiff-base Fe^{III} complexes,[6f,13,25] we can reasonably ascribe these bands to charge-transfer transitions, which necessarily overlap the metal-centered ones (especially, the $^5T \rightarrow {}^5E$ NIR absorption typical of the S = 2 Fe^{II} ion). From this study, the photoexcitation of LS Fe^{II} ions in **1** may be probed with a wavelength located in NIR, an uncommon range still selected for a few $[Fe^{II}N_6]$ compounds.[26]

Vibrational Properties. The IR spectra of **1** and **2·Solv** were recorded at RT (Figure S4 in the Supporting Information) or, in case of **1**, at variable temperature (Figure 3 and Figure S5 in the Supporting Information). The latter spectra show a broadened peak at ~1583 cm^{-1} (shoulder at 1600 cm^{-1}) indicating the coordination of Hpap-5NO_2 to the metal ion (N=C and C=C stretching vibrations).[23]

The peak at 1516 cm^{-1}, here observed at low temperature, might be indicative of a phenoxyl radical,[23,27] but we can identify at ~1285 and 1240 cm^{-1} the relatively intense signals due to the phenolato group.[23] In the spectra monitored between 233 and 363 K, it appears a number of frequencies that vary upon the spin-state switching. They are found either in the low-frequency range (582, 769, 867 cm^{-1} at 223 K, or 634, 779,

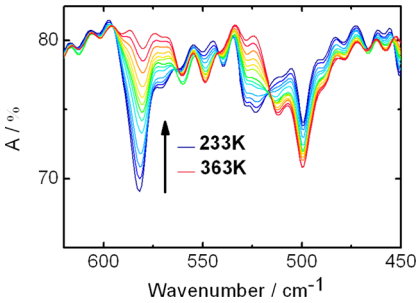

Figure 3. IR spectra of **1** (dispersed in KBr) monitored as a function of temperature between 233 (LS, deep blue), 298–311 (~T↑, green), and 363 K (HS, dark red).

810 cm^{-1} at 363 K), including the metal–ligand vibration modes or in the range dominated by the ligand-centered vibrations (1228, 1450, 1516 cm^{-1} at 223 K). The comparison between the low-frequency spectra of **1** (Figure 3) and $[Fe^{III}(pap)_2]ClO_4$[7c] confirms the absence of peaks characterizing HS (~550 and 600 cm^{-1}) and LS (~465 or 610 cm^{-1}) Fe^{III} species.

Magnetic Properties. These properties were determined from the temperature dependence of $\chi_M T$ (χ_M = molar magnetic susceptibility) of crystalline powders of **1** and **2·Solv** in the 10–400 K range. The curves in Figure 4 demonstrate the occurrence in both solids of SCO at high temperature. Remarkably, the abrupt spin transition of **1** that takes place between the S = 2 (at 400 K, $\chi_M T$ = 3.55 cm^3 mol^{-1} K) and S = 0 state (for $T \leq 80$ K, $\chi_M T \leq 0.12$ cm^3 mol^{-1} K) is centered at RT with a 17 K hysteresis (T↓ = 291 K and T↑ =

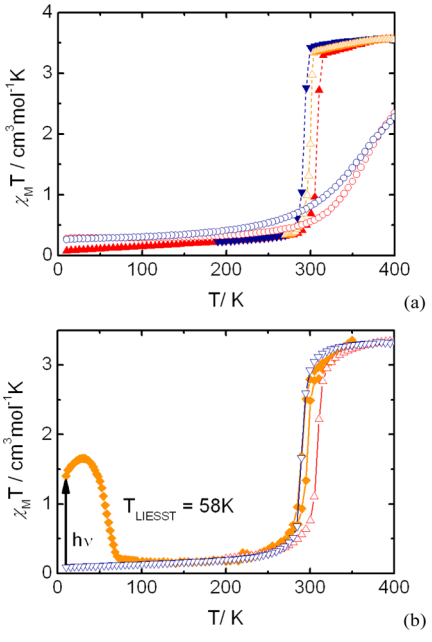

Figure 4. (a) Thermal variation of $\chi_M T$ vs T plots of polycrystalline samples **1** and **2·Solv**: upon heating (**1**, red ▲; **2·Solv**, red ○), then upon cooling (**1**, blue ▼; **2·Solv**, blue ○), and again upon heating (**1**, orange △) (sweeping rate = 2 K min^{-1}). (b) Thermal variation of $\chi_M T$ vs T plots of **1** recorded after reaching the photostationary state at 10 K with λ = 750 nm, first on heating in darkness (orange ◆), and then on cooling (orange ◆) (sweeping rate = 0.3 K min^{-1}). These curves were superimposed with the thermal behavior (red △ or blue ▽) determined for the same sample.

DOI: 10.1021/ic5027043
Inorg. Chem. 2015, 54, 1791–1799

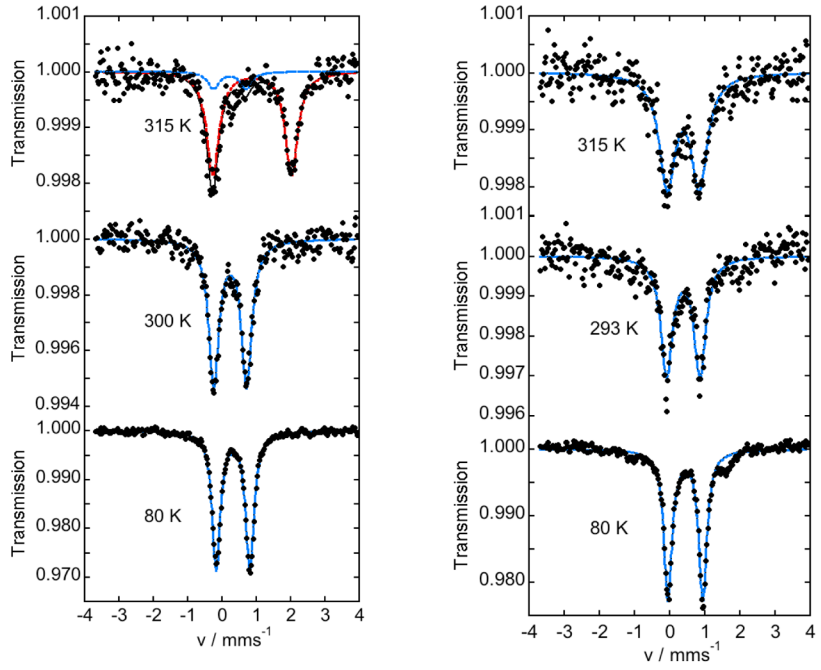

Figure 5. ^{57}Fe Mössbauer spectra of (a) Fe(pap-5NO$_2$)$_2$ recorded at 80, 300, and 315 K, (b) Fe(qsal-5NO$_2$)$_2$.2H$_2$O at 80, 293, and 315 K in the warming mode.

Table 3. ^{57}Fe Mössbauer Fitted Parameters of Fe(pap-5NO$_2$)$_2$[a]

	LS component			HS component			
T (K)	δ^{IS} (mms^{-1})	ΔE_Q (mms^{-1})	Γ (mms^{-1})	δ^{IS} (mms^{-1})	ΔE_Q (mms^{-1})	Γ (mms^{-1})	A_{HS} (%)
			Fe(pap-5NO$_2$)$_2$				
80	0.322(2)	0.981(4)	0.145(3)				0
200	0.284(6)	0.95(1)	0.155(9)				0
250	0.270(7)	0.98(1)	0.162(9)				0
300	0.238(9)	0.96(2)	0.18(1)				0
315	0.22[b]	0.95[b]	0.20[b]	0.88(2)	2.29(4)	0.22(3)	87(10)
80[c]	0.322(2)	0.971(4)	0.136(3)				0
80	0.322(2)	0.981(4)	0.145(3)				0
			Fe(qsal-5NO$_2$)$_2$·2H$_2$O				
80	0.449(3)	0.988(5)	0.141(4)				
293	0.38(2)	0.94 (3)	0.20(2)				0
315	0.38(3)	0.91(5)	0.28(4)				0
80[c]	0.431(2)	0.961(4)	0.103(3)				

[a]Isomer shifts δ are relative to Fe metal. Γ is the full width of resonance lines at half-height. The HS fraction is based on the evaluation of the areas A_{HS} and A_{LS} of the HS and LS resonance lines, assuming equal Lamb−Mössbauer factors for the two spin states. [b]Fixed during the fitting procedure. [c]Recorded after a complete thermal cycle (heating mode) and cooling.

308 K). The high- and low-temperature limits are consistent with an Fe^{II}(pap-5NO$_2$)$_2$ formulation and a complete conversion, as confirmed by the Mössbauer data. The hysteresis loop evolves upon thermal cycling of the sample in the spin-transition region (for a sweeping rate = 2 K min^{-1}: $\Delta T = T\uparrow - T\downarrow$ = 17 K upon the first cycle and ΔT = 9 K in the subsequent ones). This reflects the solid crumbling and/or the alteration of solid crystallinity (reduction of domain size, damage of long-range order) under the effect of elastic strains due to the cooperative first-order spin transition.[28]

The compound **2·Solv** shows a gradual SCO above 300 K ($\chi_M T$ = 0.50 (2.34) cm^3 mol^{-1}K at 290 (400) K). During the first thermal cycle, the sample was heated at 400 K to remove water molecules. The $\chi_M T$ versus T curve shows a similar behavior of the solvated compound except a slight shift above 200 K. We note that the value of $\chi_M T \approx 0.28$ cm^3 mol^{-1} K at 15 K may suggest the presence of traces of paramagnetic residues (including Fe^{II} or Fe^{III} metal ion). To address the issue of possible residue and to check the electronic configuration of both compounds, we performed Mössbauer measurements with exactly the same samples.

The Photomagnetic Behavior. This behavior was probed at 10 K with 750−900 nm wavelengths located in the LS charge-transfer absorption bands of **1** or **2·Solv** (Figure 2). The jump of $\chi_M T$ via the LIESST effect (Figure 4) was only detected for **1**; it was maximized with the excitation at 750 nm. The T_{LIESST} value, calculated from the minimum of $\partial(\chi_M T)/\partial T$ versus T curve, is ∼58 K, which is close to those of

DOI: 10.1021/ic5027043
Inorg. Chem. 2015, 54, 1791−1799

analogues.[10b,11a−d] The absence of any photomagnetic response for **2·Solv** suggests a rapid decay of excited states due to the high SCO temperature,[3] a too-low fraction of photoexcited species (related to the limited light penetration).[6h,29]

Mössbauer Spectra. The ^{57}Fe Mössbauer measurements (Figure 5, Table 3) were achieved between 80 and 315 K for **1** and **2·Solv**. The spectrum of **1** obtained at 80 K consists of a unique quadrupole doublet with an isomer shift of δ^{IS} = 0.322(2) mms^{-1} and quadrupole splitting of ΔE_Q = 0.981(4) mms^{-1}), that is, parameters that compare with those reported for S = 0 Fe^{II} ions in the series of [Fe^{II}(3-X,5-NO$_2$-sal-N(1,4,7,10))] compounds[19,20] (δ^{IS} = 0.33−0.46 mms^{-1} and ΔE_Q = 0.94−1.12 mms^{-1}) or a bis(pyridine-2,6-diimine)Fe^{II} complex[23] (δ^{IS} = 0.235(8) mms^{-1} and ΔE_Q = 1.081(5) mms^{-1}), a system including a potentially noninnocent ligand in a closed-shell form. No trace of paramagnetic residue was detected (amount ≤5%), and the S = 0 Mössbauer doublet was preserved up to 300 K. As established from SQUID magnetometry, an abrupt change was observed upon heating the sample within a 15 K interval. At 315 K, because of the poor statistics, the Mössbauer parameters of the LS component were fixed in coherence with the lower-temperature parameters, and the relative proportion was determined. This S = 0 quadrupole signal coexists with a new one, whose parameters (δ^{IS} = 0.88(2) mms^{-1} and ΔE_Q = 2.29(4) mms^{-1}) are typical for S = 2 Fe^{II}-(N,O) compounds (δ^{IS} = 0.82−1.07 mms^{-1} and ΔE_Q = 2.31−2.92 mms^{-1}).[19,20] This quadrupole doublet represents 87% of the total Fe content, a value that is close to the HS fraction (x_{HS}) estimated from the magnetic data (x_{HS} ≈ 92%, assuming $\chi_M T$ (Fe^{II}, S = 2) = 3.55). The 80 K data collected after this sequence confirm the sample stability. From these Mössbauer data, the S = 0 ↔ S = 2 spin-state switching exhibited by **1** may be ascribed to a spin transition of the Fe^{II} ion.

With respect to **2·Solv**, a unique quadrupole doublet was observed in the spectra at 315 and 293 K (Figure 5b). The corresponding parameters compare with the above data and move away those of [Fe^{III} (qsal)$_2$]$^+$ analogues in the S = 1/2 state (δ^{IS} = 0.06−0.25 mms^{-1} and ΔE_Q = 1.4−2.9 mms^{-1}).[30,31] This doublet is thus ascribed to a Fe^{II} ion in the S = 0 spin state. The fact that the 315 K spectrum only exhibits this doublet suggests that the content in HS species corresponds to the uncertainty of the technique, which is ca. 5%. A similar value (x_{HS} = 6% at 290 K) may be estimated from the magnetic data (assuming $\chi_M T$ (Fe^{II}, S = 2) = 3.55). At 80 K, the LS component coexists with a new doublet centered at δ^{IS} = 0.93(5) mms^{-1} that presents a quadrupole splitting parameter at ΔE_Q = 1.30(9) mms^{-1}.

The hypothesis of a sextet associated with some magnetic ordering has been ruled out by checking the spectrum recorded over a larger range of velocity. The poor statistic of the 293 K spectrum, due to the low Mössbauer resonance at high temperatures, prevents the resolution of the signal due to this impurity. However, it can be observed in this spectrum that there is some typical broadening due to the superparamagnetic fluctuation of a magnetic species.

This might suggest the presence of a HS Fe^{III}[32] or Fe^{II} contaminant, as an Fe^{II} species cannot be clearly excluded due to the typical Mössbauer parameters observed in our case (at 80 K, δ^{IS} = 0.93(5) mms^{-1}, ΔE_Q = 1.30(9) mms^{-1}). Therefore, this analysis confirms that the prevailing low-temperature signal is assignable to a LS Fe^{II} complex, and according to the magnetic data, this sample contains a small amount of HS Fe^{II} or Fe^{III} impurity.

The Ligand-Field Analysis. Of strong interest is the fact that **1**, in an unsolvated and stable form, exhibits a hysteresis loop centered at RT. From the structural analysis, the key feature for cooperativity and bistability is the strong coupling between chains of complexes and the packing as the strong electrostatic (via hydrogen bonds) and elastic interactions enhance the collective transformation of the solid. A rare result is the occurrence of SCO with Fe^{II} and Fe^{III} coordinated to the same ligand, while it is known from ligand-field considerations[33] that the considerable change (ca. 58%) in the spin-pairing energy related to the ion's electronic configurations (3d^6, 3d^5) imposes for Fe^{III} a much stronger ligand field for reaching nearly degenerate spin states. The comparison between **1**, **2**, and Fe^{III} analogues with similar conformations of ligands[6a,d,e,g,7a−c] points to the fact that a relative strengthening of the ligand field necessarily results from the orbital contractions in the 3d^5 trivalent ion.

The propensity of oxygen atom of phenol[6h] (or carbonyl[10a,c]) to establish hydrogen bonds was rarely recognized in data sets concerning such Fe^{II}/Fe^{III} materials. However, this electrostatic interaction suits for an efficient reduction of both the electronic density at the donor atoms and the ligand-field strength. Our structural analysis of **1**, **2**, and related Fe^{II}/Fe^{III} systems (Tables S1−S6 in the Supporting Information) indicates that this contribution (nonexistent in case of **2**) plays a major role in the observation of a transition of Fe^{II} in **1** (at RT) and thus favors the mismatch between the thermodynamical and interaction parameters required for a hysteretic regime. We note that these features may also account for some SCO characteristics of this important class of Fe^{III} switchable materials. Finally, the electrostatic effect in [Fe^{II}(pap-5NO$_2$)$_2$] likely prevails on the inductive effect of NO$_2$ groups, as observed from the comparison between the SCO temperatures of **2·Solv** (∼400 K) and Fe^{II}(qnal)$_2$·solvent (≤265 K).[11a]

Differential Scanning Calorimetry Data. DSC measurements of **1** (Figure 6 and Table 4; Figure S13 in the Supporting Information) reveal large enthalpy peaks (ΔH ≈ 8.5−9 kJ mol^{-1}) associated with the first-order phase transition with temperature values matching those in Figure 4. A rough estimate of entropy variation leads to ΔS values ≈ 30 J·mol^{-1}·K^{-1}, which is quite low for Fe^{II} SCO compound where the electronic contribution is $\Delta S = R \ln 5 \approx 13.4$ J·mol^{-1}·K^{-1}.[1] The feedback observed between the change of spin state and

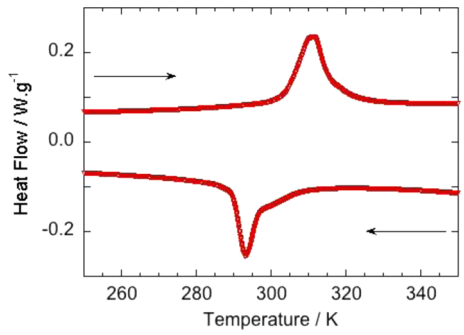

Figure 6. DSC curves of **1** recorded over the temperature range of 195−370 K (second cycle).

DOI: 10.1021/ic5027043
Inorg. Chem. 2015, 54, 1791−1799

Table 4. DSC Data and Thermodynamical Parameters for 1

mode	T_{max} (K)	T_{onset} (K)	ΔH^a (kJ mol^{-1})	ΔS (J mol^{-1}K)	$\chi_M T$ (T)^b	T (K)	$T_{1/2}{}^b$ (K)
cooling(1)	296.1	300.9	8.10		cooling(1)	291	304
heating(1)	312.4	307.1	10.30	33	heating(1)	309	
cooling(2)^c	293.1	298.3	8.90		cooling(2)	291	302
heating(2)^c	311.6	303.8	9.50	30.5	heating(2)	297	

^{a}Data corrected from the presence of 3% of HS residue. ^{b}Values extracted from magnetic measurements, in the curves of the HS fraction vs T, n_{HS} = 0.5; $T_{1/2} = (T\downarrow + T\uparrow)/2$ ^{c}Cycles 2 and 3 are identical.

hydrogen bonds might explain this observation with different and opposite phonon contributions.[34]

CONCLUSIONS

In this contribution, we have performed magnetic, Mössbauer, and structural investigations to provide evidence of SCO of Fe^{II} compounds generated with the Schiff-base ligands used in Fe^{III} spin-transition archetypes. We have shown the key importance of hydrogen-bonding interactions via the phenolate group of these ligands for varying the ligand-field strength and promoting the SCO of metal ions with a different valence, as recently described with manganese complexes.[35]

K. S. Murray has indicated, in the book edited by M. A. Halcrow,[1] the puzzling issue of "the $Fe^{II}N_2O_2{\cdot}(L)_2$ mononuclear complexes that often show more cooperative transformations than do the Fe^{II}(N-donor)$_6$ complexes". With this respect, we have demonstrated the importance of electrostatic effects whose combination with elastic properties of the lattice cause a strongly cooperative transformation of Fe(pap-5NO_2)$_2$ at RT. The examination of literature suggests that these features might also account for some SCO characteristics of this important class of Fe^{III} switchable materials.

This approach based on polar Schiff-base Fe^{II} or Fe^{III} materials is thus suitable for elaborating cooperative, bistable, and switchable systems and, more importantly, for addressing the issues of the synergy between electrostatic and elastic effects in molecular solids. One exciting development for applicative and fundamental goals (for instance in photonic and electronic research areas) is to address the size-scaling effects on such bistable molecular materials. Works in these directions are in progress.

ASSOCIATED CONTENT

Supporting Information

Further related structural data in CIF file, IR and UV−vis spectra, TGA curves, powder XRD patterns, ORTEP illustrations, and calorimetric data. This material is available free of charge via the Internet at http://pubs.acs.org. CCDC 991079−991081 contains the supplementary crystallographic data for the paper. The atomic coordinates have been deposited with the Cambridge Crystallographic Data Centre via www.ccdc.cam.ac.uk/data_request/cif. They can be obtained upon request from the Cambridge Crystallographic Data Centre, 12 Union road, Cambridge CB2 1EZ, U.K.

AUTHOR INFORMATION

Corresponding Author

*E-mail: marie-laure.boillot@u-psud.fr.

Notes

The authors declare no competing financial interest.

ACKNOWLEDGMENTS

We thank the CNRS, the French Ministry of Research, ANR (09-BLAN-0212, 12BS10006, 13-BS04-0002), and the European Regional Development Fund (FEDER) and the CEPER Nanosoft.

REFERENCES

(1) (a) Spin-Crossover in Transition Metal Compounds. In *Topics in Current Chemistry;* Gütlich, P., Goodwin, H. A., Eds.; Springer-Verlag: Berlin, Germany, 2004; Vol. *233*−*235*. (b) *Spin-Crossover Materials—Properties and Applications;* Halcrow, M. A., Ed.; John Wiley & Sons, Ltd.: New York, 2013. (c) Sato, O.; Tao, J.; Zhang, Y.-Z. *Angew. Chem., Int. Ed.* **2007**, *46*, 2152−2187.

(2) Ammeter, J. H. *New J. Chem.* **1980**, *4*, 631−637.

(3) Hauser, A. *Top. Curr. Chem.* **2004**, *234*, 155−198.

(4) (a) Kepenekian, M.; Le Guennic, B.; Robert, V. *J. Am. Chem. Soc.* **2009**, *131*, 11498−11502. (b) D'Avino, G.; Grisanti, L.; Guasch, J.; Ratera, I.; Veciana, J.; Painelli, A. *J. Am. Chem. Soc.* **2008**, *130*, 12064−12072. (c) Dei, A.; Gatteschi, D.; Sangregorio, C.; Sorace, L. *Acc. Chem. Res.* **2004**, *37*, 827−835.

(5) (a) Létard, J.-F.; Guionneau, P.; Goux-Capes, L. *Top. Curr. Chem.* **2004**, *235*, 221−249. (b) Bousseksou, A.; Molnar, G.; Salmon, L.; Nicolazzi, W. *Chem. Soc. Rev.* **2011**, *40*, 3313−3335. (c) Martinho, P. N., Rajnak, C., Ruben, M. *Spin-Crossover Materials—Properties and Applications*; Halcrow, M. A., Ed.; John Wiley & Sons, Ltd.: New York, 2013, 375.

(6) (a) Hayami, S.; Gu, Z.-Z.; Yoshiki, H.; Fujishima, A.; Sato, O. *J. Am. Chem. Soc.* **2001**, *123*, 11644−11650. (b) Dorbes, S.; Valade, L.; Real, J. A.; Faulmann, C. *Chem. Commun.* **2005**, 69−71. (c) Hayami, S.; Miyazaki, S.; Yamamoto, M.; Hiki, K.; Motokawa, N.; Shuto, A.; Inoue, K.; Shinmyozu, T.; Maeda, Y. *Bull. Chem. Soc. Jpn.* **2006**, *79*, 442−450. (d) Takahashi, K.; Mori, H.; Kobayashi, H.; Sato, O. *Polyhedron* **2009**, *28*, 1776−1781. (e) Shimizu, T.; Komatsu, Y.; Kamihata, H.; Lee, Y. H.; Fuyuhiro, A.; Iijima, S.; Hayami, S. *J. Incl. Phenom. Macrocycl. Chem.* **2011**, *71*, 363−369. (f) Tissot, A.; Bertoni, R.; Collet, E.; Toupet, L.; Boillot, M.-L. *J. Mater. Chem.* **2011**, *21*, 18347−18353. (g) Harding, D. J.; Phonsri, W.; Harding, P.; Gass, I. A.; Murray, K. S.; Moubaraki, B.; Cashion, J. D.; Liu, L.; Telfer, S. G. *Chem. Commun.* **2013**, *49*, 6340−6342. (h) Tissot, A.; Fertey, P.; Guillot, R.; Briois, V.; Boillot, M.-L. *Eur. J. Inorg. Chem.* **2014**, *1*, 101−109.

(7) (a) Hayami, S.; Gu, Z. Z.; Shiro, M.; Einaga, Y.; Fujishima, A.; Sato, O. *J. Am. Chem. Soc.* **2000**, *122*, 7126−7127. (b) Juhasz, G.; Hayami, S.; Sato, O.; Maeda, Y. *Chem. Phys. Lett.* **2002**, *364*, 164−170. (c) Hayami, S.; Hiki, K.; Kawahara, T.; Maeda, Y.; Urakami, D.; Inoue, K.; Ohama, M.; Kawata, S.; Sato, O. *Chem.—Eur. J.* **2009**, *15*, 3497−3508.

(8) Garcia, Y.; Niel, V.; Munoz, M. C.; Real, J. A. *Top. Curr. Chem.* **2004**, *233*, 229−257.

(9) Salitros, I.; Madhu, N. T.; Boca, R.; Pavlik, J.; Ruben, M. *Monatsh. Chem.* **2009**, *140*, 695−733 and references therein.

(10) (a) Weber, B.; Bauer, W.; Obel, J. *Angew. Chem., Int. Ed.* **2008**, *47*, 10098−10101. (b) Zhang, L.; Xu, G. C.; Xu, H.-B.; Zhang, T.; Wang, Z.-M.; Yuan, M.; Gao, S. *Chem. Commun.* **2010**, *46*, 2554−2556. (c) Weber, B.; Bauer, W.; Pfaffeneder, T.; Dîrtu, M. M.; Naik, A. D.; Rotaru, A.; Garcia, Y. *Eur. J. Inorg. Chem.* **2011**, *21*, 3193−3206.

DOI: 10.1021/ic5027043
Inorg. Chem. 2015, 54, 1791−1799

(11) (a) Kuroda-Sowa, T.; Senzaki, Z.; Yu, Y.; Sugimoto, K.; Maekawa, M.; Munakata, M.; Hayami, S.; Maeda, Y. *Chem. Lett.* **2008**, *37*, 1216−1217. (b) Weber, B.; Kaps, E. S.; Desplanches, C.; Létard, J.-F.; Achterhold, K.; Parak, F. G. *Eur. J. Inorg. Chem.* **2008**, *31*, 4891−4898. (c) Weber, B.; Carbonera, C.; Desplanches, C.; Létard, J.-F. *Eur. J. Inorg. Chem.* **2008**, *10*, 1589−1598. (d) Weber, B.; Kaps, E.; Weigand, J.; Carbonera, C.; Létard, J.-F.; Achterhold, K.; Parak, F. G. *Inorg. Chem.* **2008**, *47*, 487−496. (e) Zhang, L.; Xu, G. C.; Xu, H.-B.; Mereacre, V.; Wang, Z.-M.; Powell, A. K.; Gao, S. *Dalton Trans.* **2010**, *39*, 4856−4868.
(12) Clemente-Leon, M.; Coronado, E.; Lopez-Jorda, M.; Waerenborgh, J. C.; Desplanches, C.; Wang, H.; Létard, J.-F.; Hauser, A.; Tissot, A. *J. Am. Chem. Soc.* **2013**, *135*, 8655−8667.
(13) Bertoni, R.; Lorenc, M.; Tissot, A.; Servol, M.; Boillot, M.-L.; Collet, E. *Angew. Chem., Int. Ed.* **2012**, *51*, 7485−7489.
(14) Oshio, H.; Kitazaki, K.; Mishiro, J.; Kato, N.; Maeda, Y.; Takashima, Y. *J. Chem. Soc., Dalton Trans.* **1987**, 1341−1347.
(15) (a) Xie, J.-L.; Tong, W.-J.; Zou, Y.; Ren, X.-M.; Li, Y.-Z.; Meng, Q.-J. *Acta Crystallogr.* **2002**, *E58*, 334−336. (b) Takano, K.; Shibahara, T. *Chem. Lett.* **2008**, *37*, 70−71.
(16) Sheldrick, G. M. *SHELXS-97, Program for Crystal Structure Solution;* University of Göttingen: Göttingen, Germany, 1997.
(17) Sheldrick, G. M. *SHELXL-97, Program for the refinement of crystal structures from diffraction data;* University of Göttingen: Göttingen, Germany, 1997.
(18) Farrugia, L. J. *J. Appl. Crystallogr.* **1999**, *32*, 837−838.
(19) Salmon, L.; Bousseksou, A.; Donnadieu, B.; Tuchagues, J.-P. *Inorg. Chem.* **2005**, *44*, 1763−1773.
(20) Boinnard, D.; Bousseksou, A.; Dworkin, A.; Savariault, J.-M.; Varret, F.; Tuchagues, J.-P. *Inorg. Chem.* **1994**, *33*, 271−281.
(21) (a) Kuroda-Sowa, T.; Kimura, K.; Kawasaki, J.; Okubo, T.; Maekawa, M. *Polyhedron* **2011**, *30*, 3189−3192. (b) Schlamp, S.; Weber, B.; Naik, A. D.; Garcia, Y. *Chem. Commun.* **2011**, *47*, 7152−7154. (c) Kusz, J.; Nowak, M.; Gütlich, P. *Eur. J. Inorg. Chem.* **2013**, *5*−*6*, 832−842.
(22) Snodin, M. D.; Ould-Moussa, L.; Wallmann, U.; Lecomte, S.; Bachler, V.; Bill, E.; Hummel, H.; Weyhermüller, T.; Hildebrandt, P.; Wieghardt, K. *Chem.—Eur. J.* **1999**, *5*, 2554−2565.
(23) de Bruin, B.; Bill, E.; Bothe, E.; Weyermüller, T.; Wieghardt, K. *Inorg. Chem.* **2000**, *39*, 2936−2947.
(24) Haddad, M. S.; Federer, W. D.; Lynch, M. W.; Hendrikson, D. N. *Inorg. Chem.* **1981**, *20*, 131−139.
(25) Schenker, S.; Hauser, A. *J. Am. Chem. Soc.* **1994**, *116*, 5497−5498.
(26) (a) Glijer, D.; Hébert, J.; Trzop, E.; Collet, E.; Toupet, L.; Cailleau, H.; Matouzenko, G. S.; Lazar, H. Z.; Létard, J.-F.; Koshihara, S.; Buron-Le Cointe, M. *Phys. Rev. B* **2008**, *78*, 134112. (b) Buron-Le Cointe, M.; Hébert, J.; Baldé, C.; Moisan, N.; Toupet, L.; Guionneau, P.; Létard, J.-F.; Freysz, E.; Cailleau, H.; Collet, E. *Phys. Rev. B* **2012**, *85*, 064114.
(27) Itoh, S.; Taki, M.; Kumei, H.; Takayama, S.; Nagatomo, S.; Kitagawa, T.; Sakurada, N.; Arakawa, R.; Fukuzumi, S. *Inorg. Chem.* **2000**, *39*, 3708−3711.
(28) König, E.; Ritter, G.; Kulshreshtha, S. K. *Chem. Rev.* **1985**, *85*, 219−234.
(29) Enachescu, C.; Hauser, A.; Girerd, J.-J.; Boillot, M.-L. *ChemPhysChem* **2006**, *7*, 1127−1135.
(30) Nihei, M.; Shiga, T.; Maeda, Y.; Oshio, H. *Coord. Chem. Rev.* **2007**, *251*, 2606−2621.
(31) Harding, D. J.; Sertphon, D.; Harding, P. K.; Murray, K. S.; Moubaraki, B.; Cashion, J. D.; Adams, H. *Chem.—Eur. J.* **2013**, *19*, 1082−1090.
(32) (a) Vincent, J.-M.; Ménage, S.; Latour, J.-M.; Bousseksou, A.; Tuchagues, J.-P.; Decian, A.; Fontecave, M. *Angew. Chem., Int. Ed.* **1995**, *34*, 205−207. (b) Takahashi, K.; Cui, H. B.; Okano, Y.; Kobayashi, H.; Einaga, Y.; Sato, O. *Inorg. Chem.* . **2006**, *45*, 5739−5741.
(33) (a) König, E.; Kremer, S. *Theoret. Chim. Acta* **1971**, *23*, 12. (b) Hauser, A. *Top. Curr. Chem.* **2004**, *233*, 49−58.
(34) *The Hydrogen Bond;* Pimentel, G. C., McClellan, A. L., Freeman, W. H., Eds.; W. H. Freeman: San Francisco, London, 1960.
(35) Shongwe, M. S.; Al-Barhy, K. S.; Mikuriya, M.; Adams, H.; Morris, M. J.; Bill, E.; Molloy, K. C. *Chem.—Eur. J.* **2014**, *20*, 9693−9701.

DOI: 10.1021/ic5027043
Inorg. Chem. 2015, 54, 1791−1799